Characterization and Modeling of Capacitive Micromachined Ultrasound Transducers for Diagnostic Ultrasound

C.B. Doody[1], J.S. Wadhwa[2], D.F. Lemmerhirt[2], and R.D White[1]

[1]Tufts University, Medford, MA
[2]Sonetics Ultrasound, Inc., Ann Arbor, MI

ABSTRACT

This paper describes the characterization and modeling of capacitive micromachined ultrasonic transducers (cMUTs). Combining the use of finite element analysis (FEA) and lumped element modeling, computational models of the transducers were produced. Frequency response plots were generated for both transducers in air and water environments. Transient step response and frequency sweep tests were performed on single array elements using laser Doppler velocimetry. These measurements are compared to model predictions. The computational results for coupled and uncoupled arrays are compared, and show a significant increase in the array bandwidth due to coupling.

Keywords: cMUT, MEMS, FEA, LDV, ultrasound

1 INTRODUCTION

Diagnostic medical ultrasound requires arrays of ultrasound transducers for both transmit and receive operations. Most existing commercial technology uses piezoelectric crystals or piezocomposites. Capacitive micromachined ultrasound transducers (cMUTs) are a competing MEMS technology with some attractive features; particularly the possibility of integrating signal processing, signal routing, and power electronics on chip with the transducers, and also the possibility of increased bandwidth.

The design of cMUTs has been studied since the early 1990's [1]. Researchers have described a variety of cMUT designs and models [1-2]. Both lumped element modeling and finite element analysis (FEA) have been employed [3-4]. Measurements of device response often include transmit and receive frequency response measurements in a water tank, and also device input electrical impedance [1-2]. Laser interferometry has also been used in at least one case to characterize cMUT dynamics [5].

This paper presents a hybrid finite element/lumped element modeling scheme for cMUT arrays, and compares the predictions to laser Doppler velocimetry measurements. The cMUTs being tested were fabricated using layers common to standard commercial CMOS processes. For this project, two designs of micromachined ultrasonic array elements were considered.

2 MODELING

2.1 Lumped Element Modeling

In order to create a computational model of the transducers, a lumped element acoustic model was used. A coupled electrical-mechanical acoustic model of a single cMUT element can be seen in Figure 1 in transmit mode. In the model, V_{ac}, the driving RF voltage, is applied to the element's diaphragm. The output of the model is the diaphragm's volume velocity, U_{dia}. In "receive" mode an external acoustic pressure is applied to the diaphragm resulting in a volume velocity which is converted to a current by the ideal transformer, feeding from there into the receive electronics.

The lumped element acoustic model incorporates environmental loading, diaphragm mass, diaphragm stiffness, the negative electrostatic spring, and backing cavity compliance. Many of these elements were calculated analytically using known acoustic parameters [6-7].

Environmental mass loading comes from the four components for a rigid baffled piston radiating into an infinite half space for $(\omega a/c)<2$ [7],

$$R_{A1} = 0.1404\rho c / a^2 \tag{1}$$

$$R_{A2} = \rho c / \left(\pi a^2\right) \tag{2}$$

$$M_{A1} = 8\rho / \left(3\pi a^2\right) \tag{3}$$

$$C_{A1} = \left(5.94a^3\right) / \left(\rho c^2\right) \tag{4}$$

where a is the effective diaphragm radius, equal to 80% of the physical radius for a bending circular plate. ρ and c represent the speed of sound and density for the environment.

The electrostatic spring, C_{elect} is the only nonlinear element in the model, but it can be treated as a short circuit as long as the bias voltage on the transducer is not approaching the pull-in voltage. For cMUTs with a low vacuum backing cavity, the compliance of the backing cavity may not contribute much stiffness, but may be easily included,

$$C_{cav} = V_{cav} / \left(\rho_{cav} c^2\right) \tag{5}$$

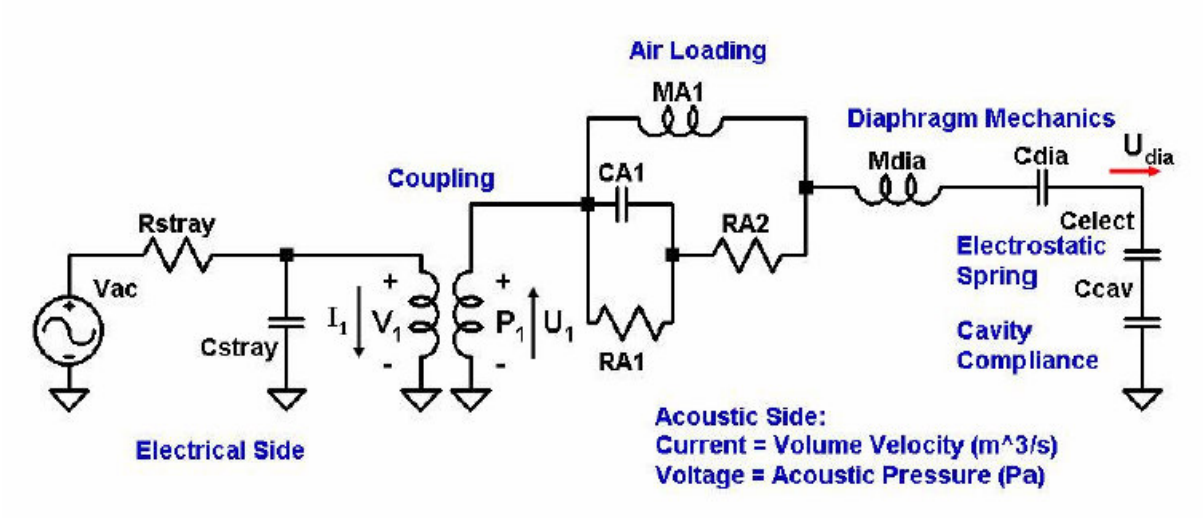

Figure 1: Mechanical-electrical lumped element model of the transducer.

where V_{cav} is the volume of the cavity, c is the speed of sound (not strongly affected by pressure), and ρ_{cav} is the density of the air in the cavity, which may be approximated by

$$\rho_{cav} = \rho_0 \frac{P_{cav}}{P_0} \tag{6}$$

where the density in the cavity is the density of air at atmospheric pressure, ρ_0, multiplied by the ratio of the cavity pressure to atmospheric pressure.

2.2 Finite Element Analysis

Due to the complex cross-sectional geometry of the transducer designs, finite element analysis was used to determine the diaphragm stiffness, effective diaphragm mass, and the electrostatic coupling for the transducer.

Using COMSOL Multiphysics ®, the geometry of each transducer was modeled as an axisymmetric cross-section. A basic layout of the transducer's cross section can be seen in Figure 2. In each case, the transducer is structured as an axisymmetric cross-section, comprised of a bulk silicon base, several thin film dielectric layers, and a passivation layer. Within the diaphragm region rests a top and bottom conductor, as well as a vacuum-filled cavity resting in between the two. The two conductive layers form the variable parallel plate capacitor for electrical-mechanical coupling. The air gap acts as a small mechanical spring.

The diaphragm acoustic compliance, C_{dia}, was calculated using a linear elastic axisymmetric static analysis. The acoustic compliance is the surface integral of the displacement in response to a unit applied pressure on the face of the transducer. An eigenfrequency analysis was then performed on the same model to determine the diaphragm effective mass, M_{dia} according to

$$\frac{1}{\sqrt{M_{dia} \cdot C_{dia}}} = f_1 \cdot 2\pi \tag{7}$$

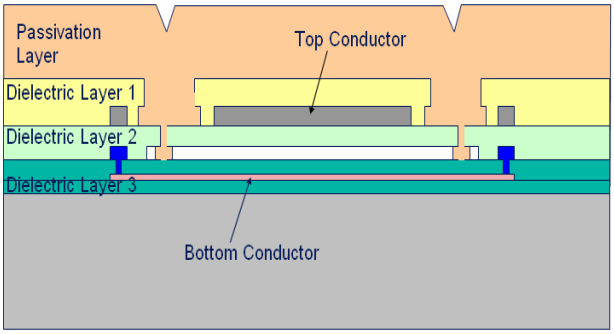

Figure 2: Axisymmetric cross-section of the transducer

where f_1 is the first eigenfrequency in cycles per second. The FEA computation was conducted for a number of different passivation layers, including PECVD nitride, Oxynitride and Parylene-C

Coupling can be computed by considering the parallel plate capacitor formed between the aluminum and the doped polysilicon with the two intervening dielectrics and the vacuum gap,

$$N = \alpha \left(\frac{d_{nom}}{\varepsilon_1} + \frac{d_2}{\varepsilon_2} + \frac{d_3}{\varepsilon_3} \right)^{-2} \cdot \left(\frac{1}{\varepsilon_1} \right) \cdot V_{bias} \tag{8}$$

where d_{nom} is the nominal height of the vacuum gap, ε_1 is the permittivity of free space, d_n and ε_n are the height and permittivity of the other intervening dielectric layers, and V_{bias} is the applied DC bias. Note that N has units of *Pa/V*, or, equivalently, *Amp/(m/s)* (in SI units). It is a bidirectional coupling constant for the ideal transformer.

Incomplete electrode coverage was handled using a nondimensional parameter α, $0 < \alpha < 1$. α is computed using

FEA as the ratio of the volume displacement obtained with a uniform unit pressure applied only on the top electrode to that obtained by applying a unit pressure over the entire face of the transducer.

With these parameters in hand, the volume velocity in response to a given DC bias plus RF drive voltage can be computed. This volume velocity can be translated into a membrane centerpoint displacement by

$$u = \frac{u_{ctr} U_{dia}}{j\omega} \tag{9}$$

where u_{ctr} is the ratio of the centerpoint displacement to the volume displacement taken from the static finite element computation. The pressure at a distance r from the element can also be estimated by treating the element as a baffled simple source, assuming we are in the farfield and there are no reflections,

$$P(r,t) = U_{dia} \frac{\rho f}{r} e^{j\omega\left(t - r/c\right)} \tag{10}$$

3 SINGLE ELEMENT RESULTS

Using the computational model, frequency response plots were generated for a single element of the array in both air and water environments. The models were also tested with different passivation layer materials and thicknesses. A sample frequency response plot can be seen in Figure 3. In air, the primary resonance for this device is predicted to be 6.1 MHz, with a very narrow fractional bandwidth of 0.2%. In the underwater environment, the model predicts a 3.4 MHz center frequency, with a fractional bandwidth of 27% for the same device. As a comparison, experimental results for transmit operation in a water tank indicate an approximate center frequency for this device of 3.3 MHz with 50% fractional bandwidth.

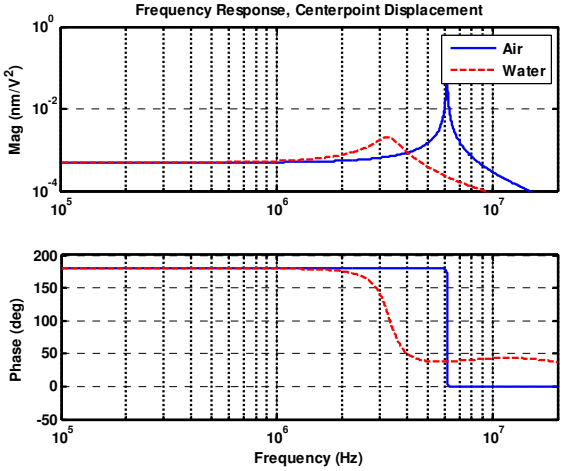

Figure 3: Modeled transmit frequency response for a single element in air and water environments.

Using LDV, a transient step response was measured for a single element in air. The result is shown in Figure 4. This is for a 0 to 10 V step. The step response shows the very high Q of the system when operating in air, and a resonant frequency of 5 MHz, similar to the high-Q 6 MHz resonance predicted by the model. The Q of the system decreases dramatically when submerged, both in computation and in water tank experiments. Model results illustrating this appear in Figure 3.

A frequency sweep test was also performed on a single element transducer, in air, with a 20 V_{PP} RF input. Due to the nonlinearity of the electrostatic drive, the transducer responds at twice the drive frequency. Test results show a peak frequency of 5.0 MHz, with an approximate 0.003 nm/V^2 low-frequency gain.

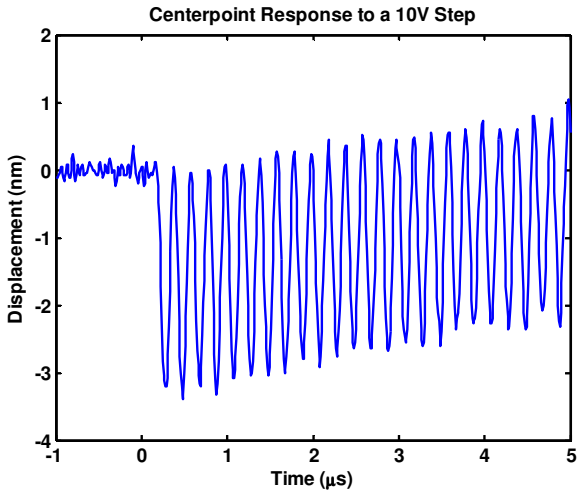

Figure 4: A 10 transient step response of a single transducer element (LDV measurement).

Centerpoint displacement calculated from the computational model was compared to the frequency sweep data obtained from the from the single cMUT element transducer. The computational model predicted a peak frequency of approximately 6 MHz, similar to the 5 MHz obtained from the transducer chip. The experimental results show somewhat larger displacements at low frequencies than the model predicts. A frequency plot comparison can be seen in Figure 5. The magnitude for the model is the amplitude of the centerpoint displacement normalized to the product of the applied DC bias and the amplitude of the RF drive voltage. For the measurement, the displacement is normalized by the RF peak voltage squared over 4, which is equivalent.

4 ARRAY COMPUTATIONS

Array computations have been carried out for a 55 element columnar array. In the coupled computation, each element is forced not only by the electrostatic force but also by the pressures generated by the motion of all other elements in the array. This leads to a matrix computation,

with a fully populated transfer function matrix including the phase lag and geometric spreading of the baffled monopole pressure field for each individual element. The array computation shows a considerable increase in bandwidth for the array over the bandwidth of an individual element. Figure 6 compares the predicted pressure for the 55 element columnar array transmitting into water at a distance 7.5 mm from the center of the array for a 40 V_p pure AC drive. The two curves in the plot represent the result when each element in the array transmits in isolation (labeled "uncoupled"), and when the fully coupled solution is computed.

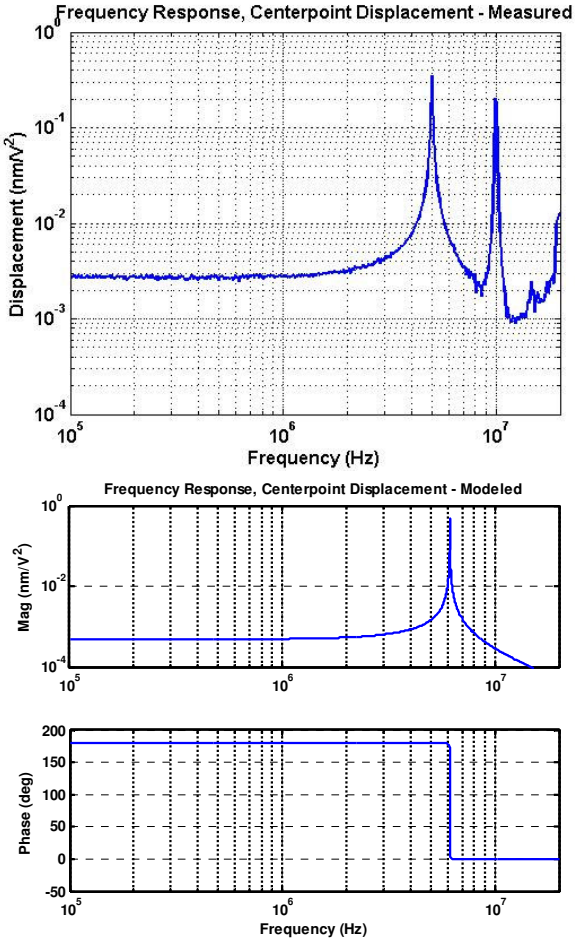

Figure 5: Frequency response comparison between computational work and experimental data.

5 CONCLUSIONS

A method of combining FEA and lumped element modeling for cMUT elements has been described. The modeling method is computationally efficient, and leads to good predictions of the resonant frequency and bandwidth of individual elements in both air and water environments. Array computations have been briefly described. The bandwidth predicted by a fully coupled computation is much wider than the uncoupled result.

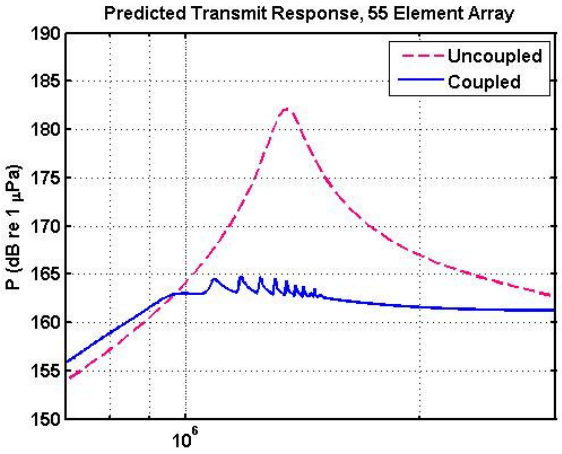

Figure 6: Comparison between coupled and uncoupled computations.

REFERENCES

[1] Ladabaum, I., Jin, X., Soh, H., Atalar, A., and Khuri-Yakub, B. *Surface Micromachined Capacitive Ultrasonic Transducers.* IEEE Transactions on Ultrasonics, Ferroelectrics, and Frequency Control, 1998, **45**(3): p. 678-690.

[2] Jin, X., Ladabaum, I., Degertekin, F., Calmes, S., and Khuri-Yakub, B. *Fabrication and Characterization of Surface Micromachined Capacitive Ultrasonic Immersion Transducers*. IEEE Journal of Microelectromechanical Systems, 1999, **8**(1): p. 100-114.

[3] Lohfink, A., Eccardt, P.-C., Benecke, W., and Meixner, H. *Derivation of a 1D CMUT Model from FEM Results for Linear and Nonlinear Equivalent Circuit Simulation*. IEEE Ultrasonics Symposium, 2003: p. 465-468 .

[4] Yaralioglu, G., Badi, M., Ergun, A., and Khuri-Yakub, B. *Improved Equivalent Circuit and Finite Element Method Modeling of Capacitive Micromachined Ultrasonic Transducers*. IEEE Ultrasonics Symposium, 2003: p. 469-472.

[5] Hansen, S., Turo, A., Degertekin, F., and Khuri-Yakub, B. *Characterization of Capacitive Micromachined Ultrasonic Transducers in Air Using Optical Measurements*. IEEE Ultrasonics Symposium, 2000: p. 947-950.

[6] Kinsler, L., Frey, A., Coppens, A., and Sanders, J. *Fundamentals of Acoustics: Fourth Edition*. John Wiley & Sons, Inc. 2000.

[7] Beranek, Leo. *Acoustics*. American Institute of Physics. 1986.